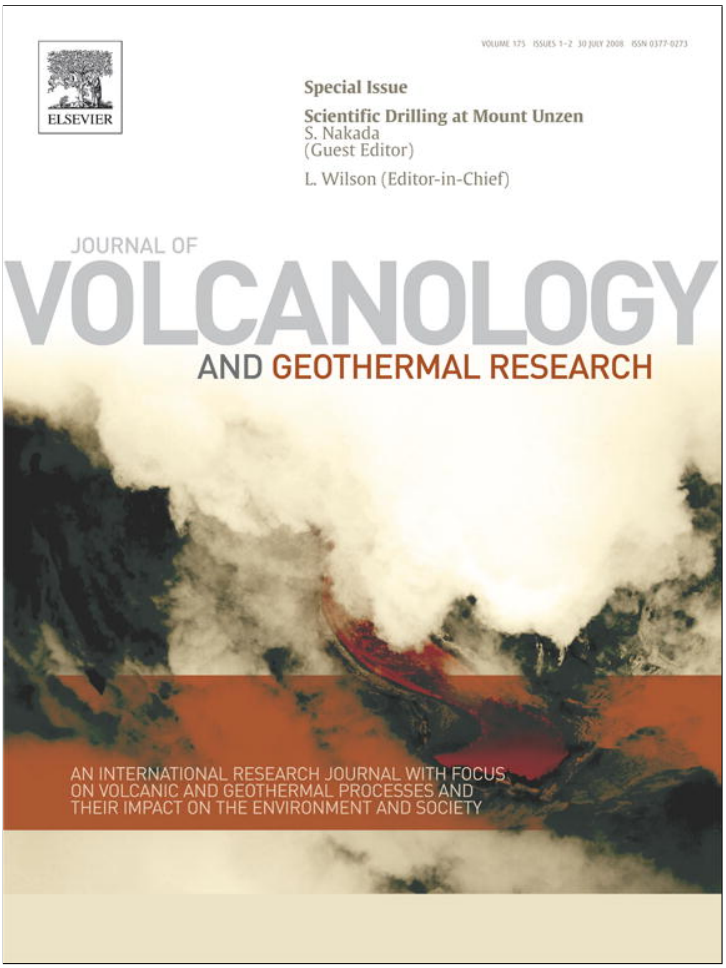

Journal of Volcanology and Geothermal Research 175 (2008) 60–70

Contents lists available at ScienceDirect

Journal of Volcanology and Geothermal Research

journal homepage: www.elsevier.com/locate/jvolgeores

Comparison of eruptive and intrusive samples from Unzen Volcano, Japan: Effects of contrasting pressure–temperature–time paths

L.D. Almberg [a,*], J.F. Larsen [a], J.C. Eichelberger [a], T.A. Vogel [b], L.C. Patino [b]

[a] University of Alaska Fairbanks Geophysical Institute, Fairbanks, AK 99775, USA
[b] Michigan State University, Department of Geological Sciences, East Lansing, MI 48824, USA

ARTICLE INFO

Article history:
Accepted 24 March 2008
Available online 12 April 2008

Keywords:
Unzen
crystallization texture
phase equilibria
decompression experiments
vesicularity

ABSTRACT

Core samples from the conduit of Unzen Volcano, obtained only 9 years after cessation of the 1991–1995 eruption, exhibit important differences in physical characteristics and mineralogy, and subtle differences in bulk chemistry from erupted samples. These differences in the conduit samples reflect emplacement under a confining pressure where about half of the original magmatic water was retained in the melt phase, maintenance at hypersolidus temperature for some unknown but significant time span, and subsequent subsolidus hydrothermal alteration. In contrast, magma that extruded as lava underwent decompression to 1 atm with nearly complete loss of magmatic water and cooling at a sufficiently rapid rate to produce glass. The resulting hypabyssal texture of the conduit samples, while clearly distinct from eruptive rocks, is also distinct from plutonic suites. Given the already low temperature of the conduit (less than 200 °C, [Nakada, S., Uto, K., Yoshimoto, M., Eichelberger, J.C., Shimizu, H., 2005. Scientific Results of Conduit Drilling in the Unzen Scientific Drilling Project (USDP), Sci. Drill., 1, 18–22]) when it was sampled by drilling, this texture must have developed within a decade, and perhaps within a much shorter time, after emplacement. The fact that all trace-element concentrations of the conduit and the last-emplaced lava of the spine, 1300 m above it, are identical to within analytical uncertainty provides strong evidence that both were produced during the same eruption sequence. Changes in conduit magma that occurred between emplacement and cooling to the solidus were collapse of vesicles from less than or equal to the equilibrium value of about 50 vol.% to about 0.1 vol.%; continued resorption of quartz and reaction of biotite phenocrysts due to heating of magma prior to ascent by intruding mafic magma; breakdown of hornblende; and micro-crystallization of rhyolitic melt to feldspar and quartz. Subsolidus changes were deposition of calcite and pyrite, growth of sericite in anorthite-rich zones of plagioclase, and development of montmorillonite as an alteration product. Significant changes in bulk composition were depletion of Mg, Fe and Na and enrichment in C and S. These changes were due mainly to the breakdown of hornblende and plagioclase, and addition of carbonate and pyrite, respectively. The identical concentrations of REEs in the conduit and surface lava are consistent with low water to rock ratios during alteration. This suggests to us that despite convective hydrothermal removal of heat from the conduit, chemical open-system effects were limited to early loss of magmatic water and later addition of magmatic CO_2 and SO_2 and/or H_2S streaming up the conduit from deeper levels.

1. Introduction

Almost two decades have passed since Unzen Volcano, Kyushu, Japan awoke from a two century-long sleep. The ensuing 4-year eruption was monitored at a level of geophysical and geochemical detail that was unprecedented at the time. These data, together with that from subsequent geophysical surveys, provided indications that the feeder system was dike-like, elongate parallel to the trend of the east–west Unzen graben within which the volcano had grown. Hoshizumi et al. (1999) documented the coincident onset of subsidence within the Unzen graben and commencement of older Unzen activity (500–200 ka) in their results from the first phase of the Unzen Scientific Drilling Project (USDP). An abrupt change in erupted lava petrology from pyroxene andesite to hybrid hornblende dacite corresponds to the change of eruption rate from the higher rate of older Unzen (500–200 ka) to younger Unzen (200–0 ka), and is thought to reflect establishment of a silicic magma chamber in the mid- to upper crust (Hoshizumi et al., 1999; Nakada and Motomura, 1999; Browne et al., 2006a).

The substantial level of understanding of the subsurface beneath Unzen from geophysical surveys, importance of the hazard that the volcano presents to society, and the ideal "end-member" status of the volcano as purely effusive despite high pre-eruption water content of the magma, led to a successful proposal to target the volcano's conduit

* Corresponding author. Tel.: +1 907 474 6171; fax: +1 907 474 5618.
E-mail address: ftlda@uaf.edu (L.D. Almberg).

0377-0273/$ – see front matter © 2008 Elsevier B.V. All rights reserved.
doi:10.1016/j.jvolgeores.2008.03.020

as part of the International Continental Drilling Program (Sakuma et al., 2008-this issue). Syneruptive degassing required to produce effusive eruptions is thought to occur in the ~1 km depth regime, so it was postulated that direct sampling and measurements in this environment would reveal how degassing occurs.

Here we describe selected features of conduit petrology and geochemistry, in comparison with erupted lava. The goal is to understand these differences in terms of the contrasting pressure (P), temperature (T), time (t) paths of magma that produced the two sample suites, as a way of elucidating the behavior of magma during shallow ascent and emplacement. Because we can only examine the end products of the extrusive and intrusive paths, a key to this understanding is replication of ascent conditions in the laboratory, with quenching and analysis of experimental charges at multiple stages along idealized paths.

2. Methods

2.1. Bulk chemistry and mineralogy analytical techniques

To determine whole rock composition, samples were cleaned in an ultrasonic cleaner with distilled water and ground by hand in an agate mortar. Three grams of this rock powder and 9.0 g of lithium tetraborate ($Li_2B_4O_7$), along with 0.5 g of ammonium nitrate (NH_4NO_3; used as an oxidizer) were fused in platinum crucibles at 1000 °C for 20–30 min on an orbital mixing stage. The melt was then poured into platinum molds, making the glass disk that was analyzed using a Bruker S-4 X-ray fluorescent (XRF) spectrograph. XRF major-element analyses were reduced by a fundamental parameter data reduction method using Bruker Spectra Plus® software, while XRF trace-element (Rb, Sr, and Zr) data were calculated using standard linear regression techniques in which the Rh Compton peak indicates mass absorption. The rare earth elements, Nb, Ta, Hf, Ba, Y, Th, U and Pb were analyzed by laser ablation inductively coupled plasma mass spectrometry (LA ICP-MS) on the same glass disks as used for XRF analyses. A Cetac LSX200+ laser ablation system was used coupled with a Micromass Platform ICP-MS, using strontium determined by XRF as an internal standard. Trace-element data reduction was done using MassLynx software. Element concentrations in the samples were calculated based on a linear regression method using well-characterized standards. Sulfur was analyzed for selected conduit and lava spine samples by XRF using pressed powders and regression techniques discussed above. All major- and trace-element whole rock analyses reported here were conducted at Michigan State University. Precision and accuracy of both XRF and LA-ICP-MS chemical analyses are reported in Vogel et al., 2006.

Dissolved inorganic carbon was analyzed using a UIC, Inc. CM5014 CO_2 Coulometer with a CM5130 Acidification Module at the University of Michigan (ASTM D513 Method B, 2002). In this method, a known amount of liquid or solid is put into a vessel that reacts with 2N H_3PO_4, allowing the release of CO_2 into a monoethanolamine solution containing a colorimetric pH indicator. As the CO_2 reacts with the monoethanolamine, a titratable acid is formed that causes the indicator to fade. Transmittance is determined on the solution. As the transmittance increases, a titration current is activated to electrochemically generate base at a rate proportional to the transmittance, until the original transmittance is obtained. Precision of the coulometer is typically less than 1%.

Mineral phases were determined using standard petrographic techniques, energy dispersive spectroscopy, and X-ray diffraction (XRD).

2.2. Porosity analysis

First-order estimations of porosity in Unzen products were calculated using single 2D slices of X-ray computed tomographic (CT) images created at the University of Texas CT facility. For the given sample size, a 1D resolution of approximately14 μm is achievable. Further work quantifying and characterizing the void volumes for the entire 3D data set is underway.

2.3. Decompression crystallization experimental procedures

We used a lightly crushed powder of the latest erupted Unzen dome material for this series of decompression crystallization experiments. The powder was loaded into 5 mm Ag tubing with sufficient distilled water to achieve water saturation. The fO_2 within the welded capsules was buffered at the NNO equilibrium under water pressure in cold-seal vessels.

A five-day equilibration at 160 MPa and 870 °C was determined empirically to be sufficient to resorb microlites into the groundmass without growing new rims on phenocrysts. Thus the starting material for the decompression experiments is a phenocryst-rich dacite with a rhyolite glass matrix, similar to the inferred post-mixing phase assemblage of Unzen magma (Holtz et al., 2005).

We ran two sets of crystallization experiments: multi-step decompression (MSD) and single-step decompression (SSD), as defined by Hammer and Rutherford (2002). The decompression rate is calculated from the pressure loss over the time since dropping the initial pressure ($\Delta P/t-t_0$), where t_0 is the time at the end of the five-day equilibration period. UNZ1-3 are MSD runs decompressed isothermally at variable rates from 160 to 7.5 MPa, to replicate a parcel of magma ascending from the shallow magma chamber to the surface. (Decompression to even lower pressures results in fragmentation of samples, therefore 7.5 MPa is used as a proxy for surface conditions.)

UZ28 is an SSD run decompressed from 160 to 40 MPa, then held for one week at the final pressure. This was done to ascertain the disequilibrium kinetic response of Unzen magma rising and stalling at the level of the USDP-4 drill hole at an averaged rate of 642 m/day (0.6 cm/s). This averaged decompression rate is within the range of plausible ascent rates of 280–730 m/day (0.3–0.7 cm/s), estimated from effusion rates (Nakada and Motomura, 1999). Plagioclase microlite nucleation and microphenocryst growth were determined in all runs by delineating regions of interest and measuring relative proportions of microlites and microphenocrysts using backscattered electron images and the NIH image-processing program ImageJ.

2.4. Plagioclase phenocryst zonation

To determine the extent of chemical zoning in plagioclase phenocrysts within the conduit, visibly zoned phenocrysts were selected for electron microprobe and LA-ICP-MS analyses from 10 thin sections cut from conduit and core samples. The analytical procedures were the same as those used by Browne et al. (2006a,b).

2.5. Resorption and reaction experimental procedures

All biotite and quartz resorption and reaction experiments were conducted by adding samples of lightly crushed Unzen spine lava to Ag capsules in the presence of 10 to 17 wt.% added de-ionized water. A small amount of water often vaporized during the final welding, leaving 9 to 16 wt.% H_2O in the charges prior to experimentation. The presence of biotite and quartz phenocrysts in the lightly crushed material provided natural “seed” crystals for the experiments. Examination of the powdered material using petrographic powders showed the presence of clean, broken biotite and quartz crystals, with little to no glass adhering to them prior to experimentation. The experimental capsules were then loaded into Waspaloy pressure vessels, with a Ni-filler rod included to buffer fO_2 at NNO+0.5 to 1 log unit. The experimental capsules were then pressurized to 160 MPa and heated to 870 °C, and held for 30 min to ensure a stable P and complete reheating of the sample. The chosen P–T conditions for the experiments replicate the estimated post-mixing, pre-eruptive P–T of the Unzen

Table 1
Major element chemistry of conduit samples compared to 1995 spine material from XRF analysis (wt.%)

Sample	SiO_2	TiO_2	Al_2O_3	Fe_2O_3	MnO	MgO	CaO	Na_2O	K_2O	P_2O_5	Totals
Uspine lava 1	65.34	0.63	15.38	4.81	0.10	2.52	4.76	3.19	2.47	0.16	99.36
Uspine lava 2	64.81	0.65	15.88	4.68	0.09	2.38	4.76	3.27	2.49	0.15	99.16
Uspine lava 3	65.32	0.61	15.74	4.57	0.09	2.32	4.79	3.30	2.43	0.15	99.32
C13-2-5C	64.05	0.63	15.27	4.61	0.10	2.07	4.85	2.79	2.44	0.17	96.98
C13-2-10	64.59	0.56	15.79	3.91	0.08	1.79	4.70	3.02	2.42	0.15	97.01
C13-2-5B	64.32	0.57	15.71	4.07	0.09	1.92	4.96	2.94	2.41	0.15	97.14
C13-4-9	65.25	0.65	15.46	3.89	0.07	1.75	4.07	2.85	2.64	0.16	96.79
C13-2-3-0~20	64.55	0.60	15.27	4.26	0.09	1.99	4.73	2.76	2.45	0.16	96.86
C14-3-10	64.01	0.58	15.78	4.13	0.07	1.43	4.61	2.84	2.49	0.15	96.09
C14-4-5	64.44	0.58	16.17	3.72	0.08	1.81	4.67	2.94	2.41	0.16	96.98
C14-2-11A	64.92	0.56	15.68	3.83	0.08	1.63	4.53	3.00	2.41	0.14	96.78
C16-3-1	63.24	0.62	14.66	4.29	0.11	2.04	4.45	2.42	2.45	0.16	94.44

Table 3
Inorganic carbon and sulfur analyses for conduit and spine samples

Sample name	wt.% inorganic carbon
C13-2-5	0.512
C14-2-11	0.386
C14-2-11 (replicate)	0.412
C14-2-11	0.254
C14-3-10	0.422
C14-4-5	0.450
Average conduit	0.406
Spine lava	0.003
	S (ppm)
C13-2-3-0~20	4800
C14-4-5	5900
Spine	280

magma (Venezky and Rutherford, 1999). The experiments were held for varying lengths of time from 6.5 to 139 h prior to quenching. Photomicrographs and some backscattered electron images were collected of the resulting experimental samples. The relative widths of reaction rims surrounding the quartz "seed" crystals were measured by outlining the areas of the rim and the "seed" crystal using reflected light images and the NIH ImageJ program.

3. Results

3.1. Chemical and mineralogical comparison of conduit and spine samples

The major- and trace-element compositions of the conduit and spine samples are presented in Tables 1 and 2, respectively. The inorganic carbon content and sulfur of selected conduit samples and the spine are presented in Table 3. Fig. 1 shows the composition of major elements in the conduit compared to the composition of the average spine sample. From Fig. 1 the relative major-element enrichment and depletion of the conduit versus the spine can be seen. Fe, Mg, and Na are depleted in the conduit with respect to the spine with the conduit to spine ratios ranging from 0.81 to 1.0 (average 0.90) for Fe; from 0.61 to 0.89 (average 0.78) for Mg; and from 0.78 to 0.95 (average 0.90) for Na. All other major elements have conduit to spine ratios near 1.0 (the averages are: Si, 1.02; Ti, 0.97; Al, 1.02; Ca, 1.00; K, 1.03; P, 1.04).

Inorganic carbon concentration in the conduit sample ranges from 0.25 to 0.50 wt.% C, averaging 0.41%, whereas the spine sample is near or below detection limits (0.003 wt.% C). Sulfur concentrations in the conduit sample were 4800 to 5900 ppm, whereas in the spine they were 280 ppm.

Fig. 2 shows spider plots of rare earth elements and other trace elements in the conduit and spine. In these plots, there is no difference between the conduit and the spine samples. To further aid in this comparison, a plot of the ratio of the average conduit to the average spine is shown in Fig. 3. It can be seen from this figure that all differences in concentrations are within analytical precision (10%).

The textural and mineralogical differences between Unzen conduit and dome samples are apparent and striking both in hand specimen and thin section. Phenocryst phases abundant in Unzen eruption products, plagioclase, hornblende and biotite, are extensively altered, recrystallized, and/or replaced in conduit samples. We also find conspicuous variations in mineralization across the spectrum of samples retrieved from the USDP-4 drill core. Our discussion is based on analyses of core samples C14-2-11 and C16-2-2, which we were able to investigate in detail, and the spine lava, which was the last-extruded lava.

Unzen lava samples contain 20–30% euhedral phenocrysts of plagioclase, hornblende, biotite, magnetite, ilmenite and minor embayed quartz set in a microlite-rich groundmass (Fig. 4; Nakada and Motomura, 1999). Plagioclase is the most abundant phase and is present as microlites (<20 μm, longest dimension), microphenocrysts (20–100 μm) and complexly zoned phenocrysts (>100 μm; Browne et al., 2006b). Pyroxenes and plagioclases occasionally occur together as crystal clots. All are set in clear, colorless rhyolitic glass (Nakada and Motomura, 1999), which constitutes 50–70 vol.% of the groundmass.

In contrast, conduit samples have altered or decomposed phenocrysts set in completely crystalline groundmass. Plagioclase phenocrysts in the conduit are similar in appearance to plagioclase phenocrysts in lava, but anorthitic zones are sericitized. Plagioclase microphenocrysts are absent in the conduit (Fig. 4). Diffuse sericite masses are dispersed throughout. Pseudomorphs of calcite and chlorite after hornblende are common, as seen in Fig. 4. Biotite is abundant both as unaltered, broken phenocrysts and partially altered phenocrysts. Chloritized biotites, sometimes with reaction rims, are typically found adjacent to sericitized plagioclase phenocrysts. Additional crystal phases identified in samples retrieved from depth

Table 2
Trace-element chemistry of conduit samples compared to 1995 spine material (ppm)

Sample	Cr	Rb	Sr	V	Y	Zr	Nb	Ba	La	Ce	Pr	Nd	Sm	Eu	Gd	Tb	Dy	Ho	Er	Yb	Lu	Hf	Ta	Pb	Th	U
Uspine lava 1	52	77	288	154	17.6	128	16.3	437	20.87	43.04	4.44	15.62	3.36	0.94	3.63	0.55	2.89	0.63	1.86	2.04	0.30	3.15	1.17	14.70	9.30	3.30
Uspine lava 2	26	79	307	160	14.9	129	16.2	466	20.51	40.99	4.15	14.52	3.12	0.94	3.42	0.49	2.62	0.56	1.69	1.92	0.27	3.11	1.17	15.63	9.08	3.37
Uspine lava 3	49	76	306	164	15.3	119	16.0	460	21.16	43.47	4.37	14.76	3.37	0.98	3.50	0.51	2.70	0.59	1.75	2.07	0.29	2.93	1.21	16.59	9.36	3.63
C13-2-5C	58	75	313	160	15.9	140	16.4	487	20.86	43.36	4.42	15.39	3.39	0.95	3.61	0.53	2.77	0.59	1.76	1.99	0.29	3.32	1.19	17.77	8.65	3.38
C13-2-10	48	73	334	137	13.1	116	15.0	492	19.05	39.10	3.91	12.99	2.99	0.88	3.08	0.47	2.40	0.54	1.75	1.77	0.24	2.82	1.19	18.92	8.43	3.25
C13-2-5B	46	74	335	132	13.9	124	15.2	475	19.56	39.31	3.99	13.70	2.88	0.91	3.04	0.48	2.46	0.53	1.61	1.80	0.27	3.00	1.14	17.80	8.62	3.08
C13-4-9	40	82	321	159	14.3	125	17.3	556	20.96	42.55	4.22	14.40	3.19	0.89	3.31	0.47	2.59	0.59	1.73	1.89	0.26	3.03	1.29	20.96	9.53	3.51
C13-2-3-0~20	38	74	309	145	14.5	120	15.9	500	20.83	43.33	4.31	14.54	3.20	0.95	3.42	0.52	2.62	0.56	1.71	1.92	0.26	3.02	1.21	17.70	9.23	3.38
C14-3-10	51	74	354	125	14.9	136	15.3	481	21.12	41.68	4.30	14.93	3.03	0.91	3.38	0.49	2.58	0.56	1.74	1.93	0.27	3.31	1.20	16.82	9.51	3.06
C14-4-5	55	70	347	121	15.7	141	15.0	474	21.72	41.88	4.30	15.20	3.10	0.94	3.38	0.49	2.64	0.56	1.75	1.95	0.27	3.29	1.19	16.16	9.70	2.88
C14-2-11A	29	74	346	110	14.2	136	14.6	483	21.08	39.91	4.13	13.97	2.94	0.95	3.20	0.49	2.48	0.53	1.62	1.84	0.26	3.37	1.20	16.63	10.03	2.95
C16-3-1	51	71	288	118	16.3	140	15.1	446	21.45	42.61	4.42	15.42	3.24	0.97	3.63	0.53	2.79	0.61	1.82	2.04	0.28	3.41	1.20	16.94	9.93	2.81

Chromium, Rb, and Sr from XRF analysis, all others from ICP-MS analys.

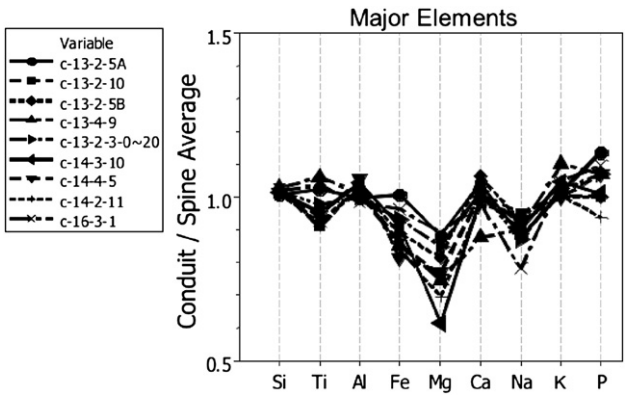

Fig. 1. Whole rock conduit/spine ratios for major elements. Note the depletion in Fe, Mg and Na.

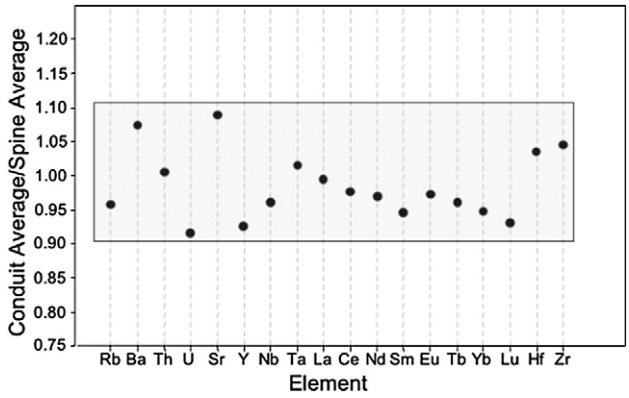

Fig. 3. Trace elements in the conduit/spine. The gray area is a conservative estimate of the analytical precision. Much of the variation is below this precision level. The conclusion is that there is no difference in the trace elements from the conduit and spine.

include pyrite, apatite, zeolites, calcite, oxides, K-feldspar and minor zircon and sphene. Pyrite occurs both as small grains disseminated through the groundmass and concentrated along microfractures.

The groundmass of the conduit is wholly crystalline, comprised of a felted mass of clear crystals of quartz and K-feldspar (Fig. 4). We find quartz as a groundmass phase only, not as quartz phenocrysts (Fig. 5). This is in contrast to lava, where partially resorbed quartz phenocrysts are a minor but ubiquitous component. Despite the visual prominence of quartz in lava, it is not detected in XRD data, whereas the dispersed quartz of the conduit matrix is displayed in the XRD diffractogram (Fig. 5).

3.2. Decompression crystallization results

It has previously been recognized that water pressure has a large effect in suppressing the plagioclase liquidus and shifting plagioclase–melt equilibrium towards more calcic compositions. Consequently, water loss from melt during decompression promotes rapid crystallization of relatively sodic plagioclase (Cashman and Blundy, 2000). We have examined this behavior for Unzen magma in reconnaissance fashion in order to view decompression crystallization at various rates of nearly complete decompression and upon emplacement at the sampling depth of the conduit (Fig. 6).

Qualitative assessment of the MSD experiments indicates that plagioclase microlite crystallinity is negatively correlated with decompression rate — faster decompression of experiments yields lower crystallinities. The three MSD experiments UNZ1 (2.1 MPa/h), UNZ3 (1.1 MPa/h), and UNZ2 (0.7 MPa/h) developed crystallinities of 1.89±3.0%, 2.13±1.5%, and 5.86±2.1%, respectively, based on the weighted average analysis of three BSE images per sample. UNZ1 is more heterogeneous than the other MSD experiments, thus the groundmass crystallinity is not significantly different than UNZ3 within 1σ. Groundmass plagioclase crystallinity in UNZ2 is, however significantly greater than in UNZ3. The characteristic microlite size increases systematically with decreasing average decompression rate for these three MSD experiments: 2.18±1.2 μm (UNZ1), 2.81±0.9 μm (UNZ3), 3.66±0.9 μm (UNZ2). The large range of crystal sizes found in each experiment, however, precludes us from finding a significant difference between the characteristic crystal sizes in these three experiments. The volume density of microlites (log number per mm^3) also increases with slower decompression: 5.73±0.4 (UNZ1), 5.96±0.2 (UNZ3), 6.09±0.2 (UNZ2), yet UNZ2 is not significantly greater than UNZ3 within error.

3.3. Plagioclase zonation

Although they are similar in appearance, a remarkable chemical contrast between plagioclase phenocrysts from the conduit to those from the surface samples exists. In particular, there is an absence of extreme excursions in anorthite concentration and Sr/Ba that is evident in plagioclase from the surface samples. Fig. 7 shows an example of a clear, high An outer rim on the plagioclase, which is similar to those that occur in plagioclase phenocrysts in the spine discussed above. Rims with higher An content are observed in the conduit, but they are not common and do not have as high An content as observed in the spine plagioclase. More commonly, the clear rim on plagioclase in the conduit has a composition similar to the interior of the plagioclase in both An content and Sr/Ba ratio.

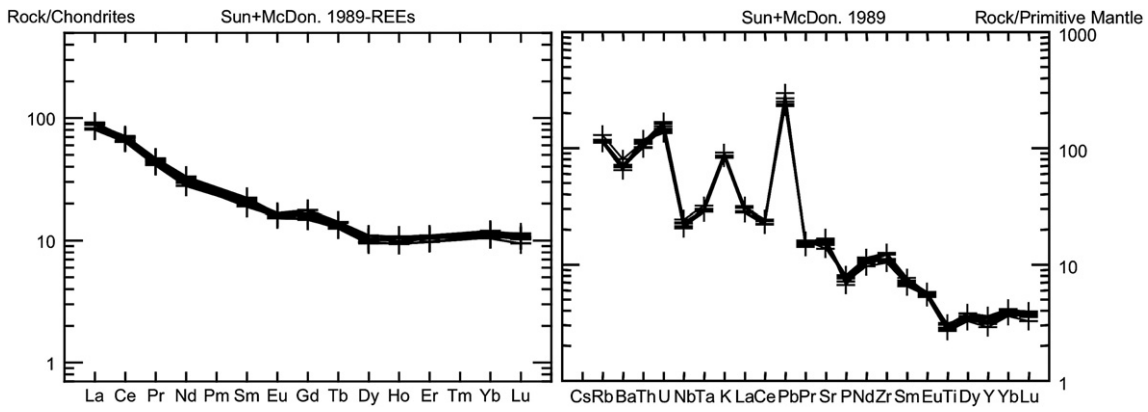

Fig. 2. A) Rare earth element diagrams and B) Spider diagram for select trace elements for all of the samples. Samples normalized to chondrites using values from Sun and McDonough (1989). Note that there is little variation among the samples and that the conduit and spine samples are identical.

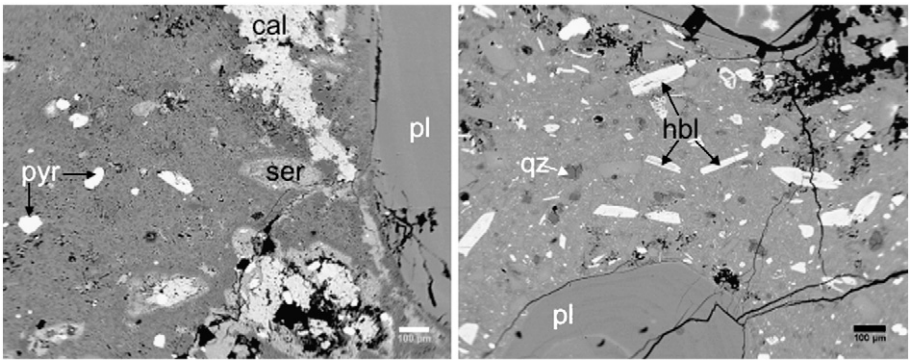

Fig. 4. Backscattered electron images of intrusive and extrusive textures. Conduit sample (left) (C14-2-11) exhibits granophyric texture with felted mass of crystals in groundmass and some diffuse areas of sericite that may be relicts from plagioclase microphenocrysts. There is no glass. Spine lava (right) has prominent microphenocrysts of plagioclase set in microlite-rich clear rhyolite glass. Mineral abbreviations: pl — plagioclase, hbl — hornblende, pyr — pyrite, ser — sericite, cal — calcite, qz — quartz.

3.4. Resorption and reaction experimental results

It was found that quartz is not stable under the post-mixing, pre-eruption conditions of 870 °C and P_{H2O} = 160 MPa, inferred by Venezky and Rutherford (1999). Reaction rims surrounding quartz phenocrysts in enclaves in samples from the 1995 lava are predominantly augitic pyroxene (clinopyroxene), with smaller amounts of hornblende and orthopyroxene (Fig. 8, sample 26255-eUSDP; Sato, pers. comm., 2006). The reaction rims that formed around quartz in the experiments are also predominantly Ca-rich clinopyroxene, with minor orthopyroxene present as well. They appear to lack hornblende, which could reflect a more sluggish crystallization rate for that phase. However, while the reaction rims are always present in the experiments, they are sometimes absent in the natural samples, with the phenocrysts showing resorption only (Fig. 8). Reaction rims are always observed on quartz included within mafic enclaves. Quartz showing resorption without reaction rims occurs primarily in the host magma (Browne et al., 2006a).

The experiments also show that pyroxene reaction rims form around the quartz "seed" crystals after as little as 6.5 h (Fig. 8). Fig. 9 shows the proportion of the rim area to the area of the partially resorbed quartz seed crystal as a function of time. The rim areas reach approximately 70% of the area of the seed crystal after about 25 h, and then generally plateau in runs up to the maximum duration of ~140 h. No experiments resulted in complete elimination of quartz by reaction with melt.

4. Discussion

4.1. Bulk chemistry and mineralogy

The differences in chemistry between the conduit and the spine are depletion of Mg, Fe and Na, and enrichment of C and S (Fig. 1 and Table 3). All of the other major elements are similar in the conduit and spine (Fig. 1). The depletion of Mg is very large in some samples (nearly 40% depleted, Fig. 1). Fe and Na depletions are not so extreme and in some conduit samples they are not depleted or only very slightly depleted (Fig. 1). The rare earth elements (REEs) and other trace elements are nearly identical in the samples from the spine and those retrieved from depth (Figs. 2 and 3), leading us to conclude that they are likely from the same eruptive sequence.

The depletion of Mg and Fe is consistent with the breakdown of hornblende with some of the Mg and Fe being mobilized in the conduit. The depletion of Na is consistent with the breakdown of plagioclase and mobilization of Na. The large increase in C and S in the conduit compared to the spine (Table 3) is consistent with addition of CO_2 and SO_2 during hydrothermal alteration, which resulted in the formation of calcite and pyrite in the conduit and retention of Ca and some of the Fe in the system. The Ca in calcite most likely was produced by breakdown of plagioclase and hornblende, whereas the Fe in pyrite was from the breakdown of hornblende. The abundance of carbon and sulfur in the conduit samples is most likely due to magmatic CO_2 and SO_2 streaming upward as magmatic gas from deeper in

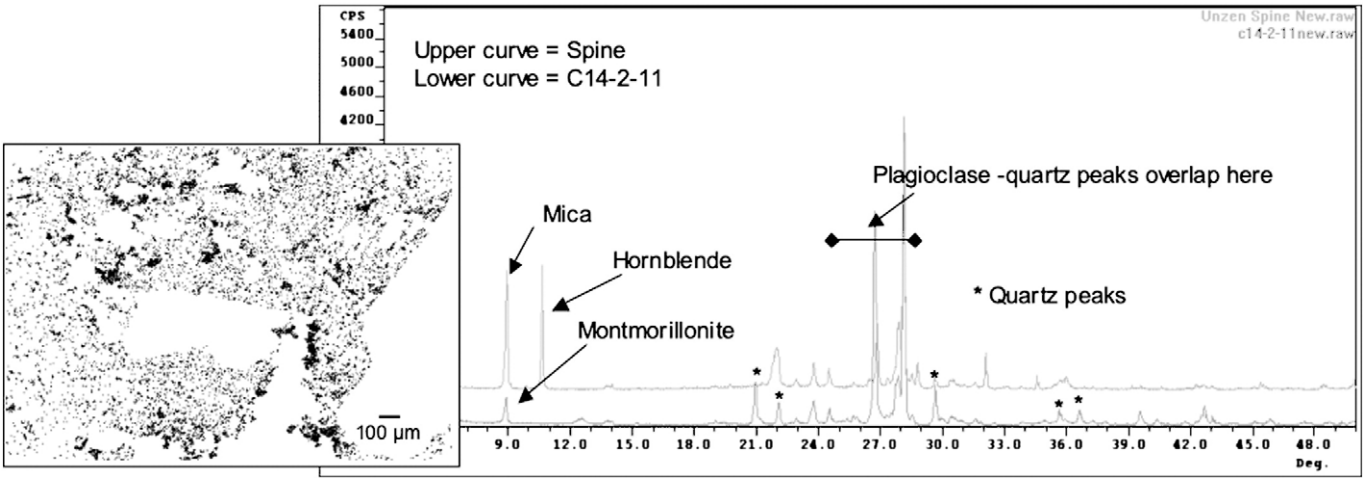

Fig. 5. Quartz in Unzen conduit. (Left) black areas of X-ray map image of conduit sample are rich in Si with S, Mg, Al, Ca, and K absent and are therefore presumed to be SiO_2. (Right) XRD diffractogram showing quartz lines in conduit.

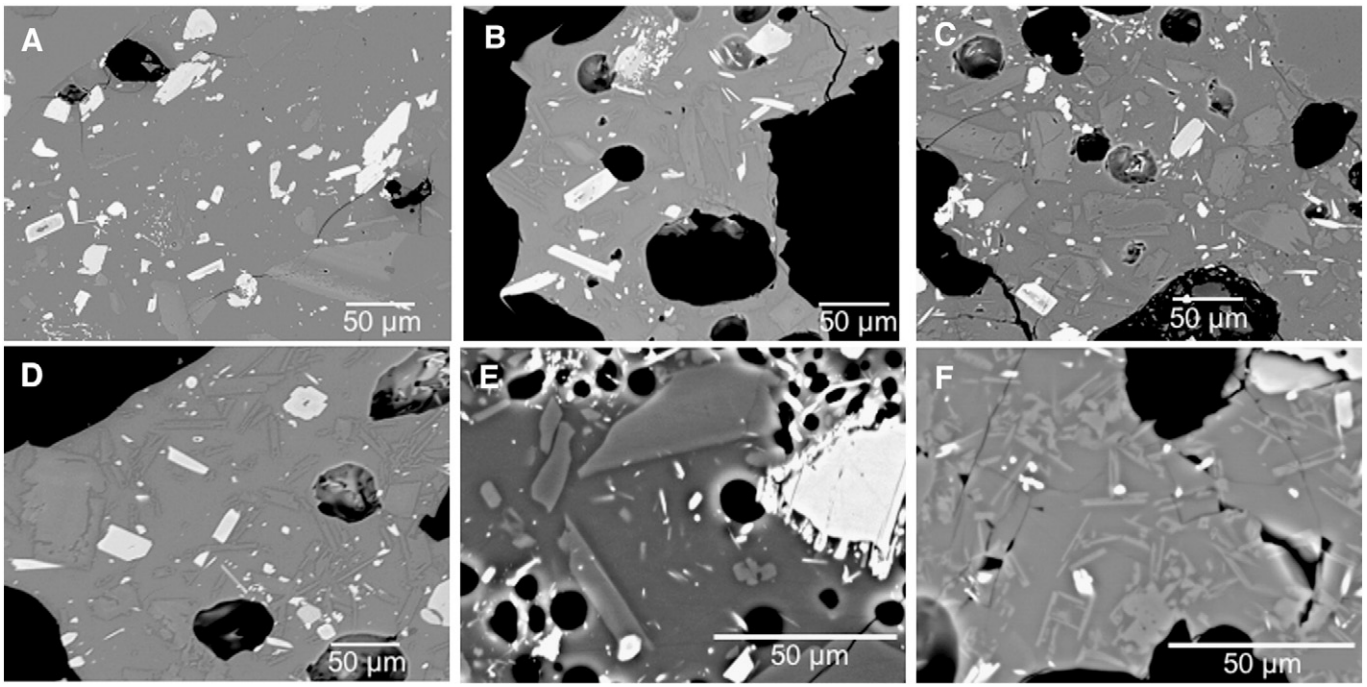

Fig. 6. Backscattered electron images of experimental runs: A) UNZ4 — Unzen dacite held at inferred pre-eruption conditions (160 MPa, 870 °C) for 139 h; B) UNZ1 — equilibrated as (A) then decompressed at 2.1 MPa/h to 7.5 MPa; C) UNZ3 — decompressed at 1.1 MPa/h to 7.5 MPa; D) UNZ2 — decompressed at 0.7 MPa/h to 7.5 MPa; E) UZ28 — decompressed ~instantaneously and held at 40 MPa for one week; F) UZ29 — decompressed ~instantaneously and held at 40 MPa for 48 h.

the system. Given their abundance and negligible (CO_2) to low (SO_2) solubility in silicic melt at mid- to upper crustal depths, their ultimate source is likely recently intruded mafic magma as indicated by the presence mafic enclaves in the lava (e.g., Browne et al., 2006a).

The closely similar REE and other trace-element concentrations of the conduit and spine lava samples from Unzen seem surprising given the pervasive hydrothermal alteration. With respect to the REEs, we can therefore infer that the hydrothermal alteration that affected the conduit happened under conditions where REE-hosting phases were stable. Fulignati et al. (1998) evaluated REE mobility in hydrothermally altered rocks and concluded that the mobility of REEs was related to pH. In neutral or high pH and low water/rock ratios result in low mobility (Ayers and Watson, 1991; Fulignati et al., 1998). The solubility of REE-hosting phosphates, e.g. monazite, has been extensively

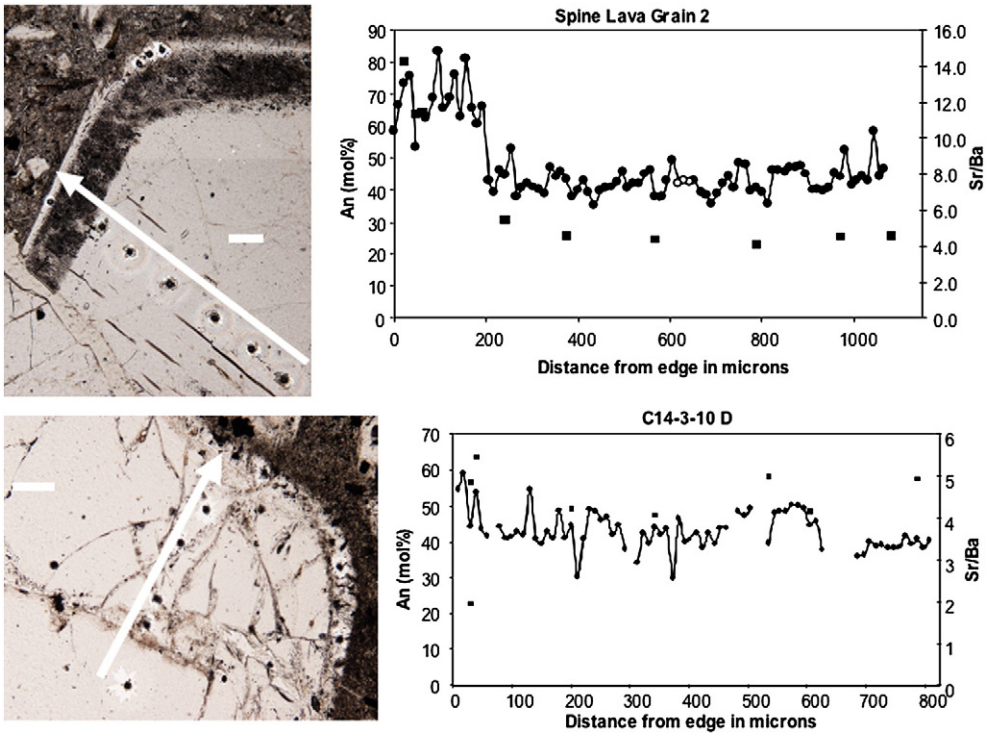

Fig. 7. Superimposed An and Sr/Ba versus radial distance profiles for plagioclase phenocrysts in spine lava (top) and conduit sample C14-3-10 (bottom).

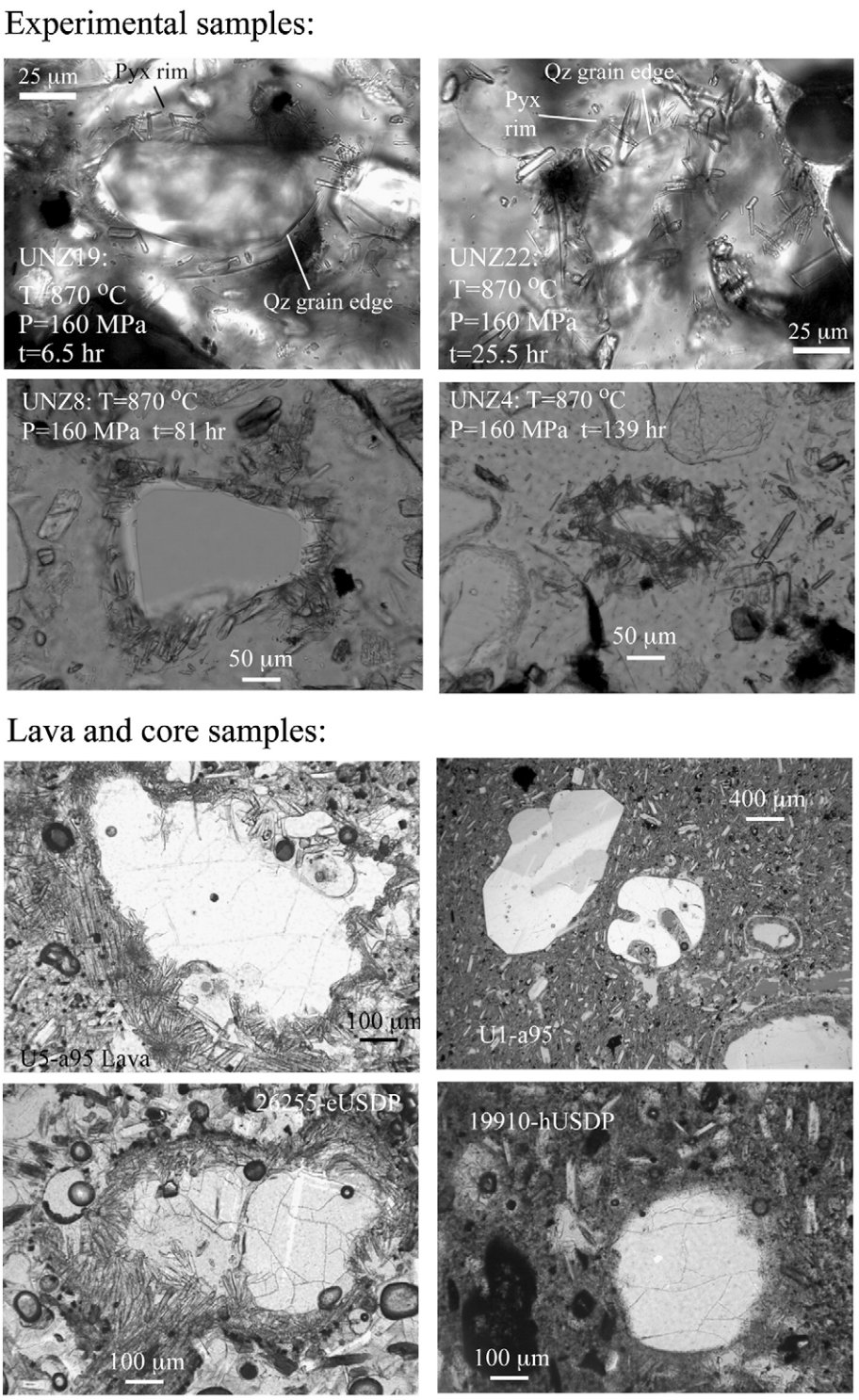

Fig. 8. The four photomicrographs at the top of this figure show the progression of quartz reaction rim textures as a function of experiment duration. The pressure and temperature conditions are listed on each photomicrograph, along with the run number. These images show that the rims develop rather quickly, over a ~24 hour period, when the Unzen natural powder starting material is subjected to the estimated post-mixing temperature of 870 °C. The lower four photomicrographs show the range of quartz textures observed in the Unzen samples from flank drill core samples, as well as the spine lavas. The two images on the left show well-developed augite reaction rims, while those on the right show resorption only without augite reaction rims.

studied at <300 °C (e.g. Cetiner et al., 2005). It has been concluded that, at near-surface conditions, the stability of these phases depends mostly on temperature, pH, ligands present, and water/rock ratio (Wood and Williams-Jones, 1994; Gammons et al., 1996; Cetiner et al., 2005). Monazite is less stable at low temperatures and low pH (Cetiner et al., 2005). In fact, pH seems to be the most important parameter; the solubility of REE-hosting phosphates increases with decreasing pH. Our understanding of the stability of REE-hosting phases at higher *P* and *T* is more limited. However, Ayers and Watson (1991) reach similar conclusions regarding the importance of pH in the stability of apatite and monazite at higher *T* (800–1200 °C) and *P* (1.0–3.0 GPa). At these conditions, the solubility of apatite is not

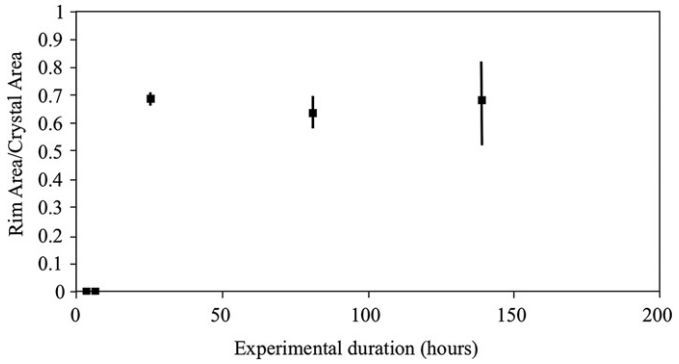

Fig. 9. Ratio of rim area to remaining area of the associated "seed" crystal, as a measure of the quartz+melt to augite reaction plotted against experimental duration. Error bars represent the standard deviation about the mean areas measured. Development of the reaction rims is rapid, occurring primarily within the first 24 h of each experiment.

affected by temperature, but the solubility of monazite increases with increasing temperature if the pH is low. Based on this information, the pH may have been sufficiently high to prevent breakdown of REE hosts, such as apatite and zircon, and transport of the REE out of the system or the solution had low pH but it interacted only with a small portion of the rock.

We infer from the presence of matrix quartz but absence of phenocrystic quartz in the conduit that resorption of quartz was occurring during the eruption and went to completion because conduit magma stayed at high temperature for a significant time after emplacement, only to be re-precipitated during eutectic-like crystallization of the magma's matrix rhyolite. In the lava, cooling occurred before resorption of quartz phenocrysts was complete, and before the melt could begin to precipitate quartz.

4.2. Decompression crystallization

The SSD experiments yield heterogeneous results and do not conform to the nucleation and growth curve of the MSD experiments (e.g. Fig. 6E shows a less crystalline area of the experimental charge than Fig. 6F, although 6E represents a longer experiment). Hammer and Rutherford (2002) demonstrated that this is to be expected and indicated that MSD series are more appropriate to approximate the slow, steady decompression accompanying a dome-forming eruption. Couch et al. (2003b) found that for experiments with similar compositions and initial conditions decompressed to 50 MPa, crystallization begins after 1 h and stabilizes within 4–8 h. Holding these experiments at 40 MPa for 48 h and one week, with an effective undercooling of ~150 °C (Couch et al., 2003a) produced low crystallinity (3–9%) for a decompression rate close to that inferred by Nakada and Motomura (1999). The quantitative data available at this time are too limited to make more detailed comparisons to the analyses of natural and experimental samples for Mount St. Helens (Cashman, 1992, Geschwind and Rutherford, 1995) and Mount Pinatubo (Hammer et al., 1999). The final results of this decompression crystallization study will be presented in a subsequent paper.

4.3. Porosity

Porosity of eruption products is the first-order evidence that magmas contain volatiles that exsolve upon decompression. Ideally, porosity of tephra, lava, and conduit samples might be assumed to equal volume fraction of vapor at the time of eruption or emplacement if the material has been rapidly quenched. In reality, this ideal case is only approached in explosive events (e.g., Klug and Cashman, 1994, Thomas et al., 1994, Klug et al., 2002, Polacci et al., 2003, etc.). Primary porosity, or vesicularity, is lost when lithostatic pressure is constant (decompression stops) and the temperature of magma or volcanic deposit remains above the glass transition temperature for an extended period. During this time, bubbles formed during the previous decompression step can continue to coalesce, providing pathways for degassing and ultimately bubble collapse as well as resorption of residual vapor into the melt. This effect is greatly enhanced when the material is under mechanical load, as in lava flows and conduits, and is well understood in the case of ignimbrite sheets, where it is called "welding" (e.g., Riehle, 1973).

Assuming initial water content in the magma of 5–7 wt.% H_2O (Moore and Carmichael, 1998; Holtz et al., 2005, Nishimura et al., 2005), that the gas expands ideally, and that the system is closed to gas loss gives 40 vol.% vesicularity at 1.3 km depth. Even if all this gas escapes, secondary porosity will later be generated through second boiling as the melt crystallizes. Because sampled conduit material was emplaced under pressure sufficient for 2.6 wt.% H_2O to be retained in melt, this is a significant effect that would yield another 43 vol.% vapor at equilibrium in a closed system conduit. If fluids flux through the emplaced magmatic material, porosity can potentially be further changed under appropriate *P*/*T* conditions.

A simple 2D analysis of void space ratios in conduit yields vesicularities of 0.01–0.3 vol.% in conduit samples and 3.3 vol.% in spine samples. It is clear, even from the simplistic approach taken here, that the remnant vesicularity is one or two orders of magnitude less than that expected from an ideal gas expansion model for the dome and conduit samples, respectively. The obvious inference to be drawn is that gas loss has been highly efficient and essentially complete. For this to occur, the conduit magma had to retain some permeability down to very low porosity. Gas pathways once established must persist despite bubble collapse.

4.4. Zoning in plagioclase phenocrysts

Browne et al. (2006a,b) showed that strong anorthite–albite zonation in plagioclase phenocrysts was accompanied by strong variation in Sr/Ba. There is an outward progression from low An, low Sr/Ba through a sieve-texture resorption zone to thin, strongly normally zoned high An, high-Sr/Ba to low An, low Sr/Ba rim. This reflects both chemical and thermal perturbations to the crustal magma system caused by injection of basalt, followed by reestablishment of equilibrium. Indeed, the plagioclase phenocrysts appear to have been actually engulfed in intruding basalt and then recycled back into the host silicic magma. We extended this study of plagioclase zonation to conduit samples and found that zoned phenocrysts lacked the high An, high-Sr/Ba peak of the outer rim (Fig. 7).

Two explanations may be considered for the lack the An-spike in plagioclase phenocrysts retrieved from 1.3 km depth. This zone may never have developed due to a lesser amount admixed mafic magma or because the conduit samples were emplaced early in the eruption sequence, eliminating a post-mixing equilibration period in which new rims could grow. Alternatively, the rims could have been eliminated by diffusion. For diffusion to have erased the high An signature, it would require diffusion coefficients for Ca–Na on the order of 10^{-10}cm^{2}s^{-1} active over the 10–15-year period after emplacement, which are higher than the diffusion coefficients measured under wet conditions at 900 °C by Liu and Yund (1992). Using their diffusion coefficients, a 10-μm characteristic diffusion distance would occur in 10 years. However diffusion experiments are very sensitive to temperature, composition of the liquid and crystal and the presence of volatiles. Still, it is not probable that the diffusion rates were 1 to 2 orders of magnitude faster in the conduit than measured under Liu and Yund's experimental conditions, especially given that the magma cooled by several hundred degrees in the years following emplacement. The fact that texturally these rims on zoned phenocrysts in the conduit appear similar to the rims in the effused lavas without the accompanying high An content may be coincidental, leaving open the question of how they formed.

4.5. Resorption and reaction of biotite and quartz phenocrysts

Unzen magma was affected by three major perturbations to its equilibrium storage conditions just prior to and during eruption. One was coupled heating and compositional change due to input of basaltic magma (Nakamura, 1995; Venezky and Rutherford, 1999; Browne et al., 2006a). Next was decompression due to ascent. Finally, there was slow to rapid cooling depending upon whether the magma was emplaced in the conduit or on the surface. As a consequence, biotite and quartz phenocrysts in lava and conduit samples exhibit resorption and reaction relationships with the host melt as represented in samples by glass or matrix. The extent to which these processes proceeded differed between the conduit and lava samples.

4.5.1. Quartz

The likely cause of reaction and resorption of quartz phenocrysts in Unzen magma is heating above the temperature stability limit of quartz, which is about 780 °C at 160 MPa (Holtz et al., 2005). The experimental timescale of 1 day to produce the rims around the quartz seed crystals is shorter than the time inferred to have elapsed between magma-mixing and eruptive quenching based on titanomagnetite diffusion profiles, 11–29 days (Venezky and Rutherford, 1999) and is even shorter than the shortest timescale, 7 days, inferred for magma ascent (Nakada and Motomura, 1999). Thus, it is likely that the rims formed primarily during initial contact between stored silicic magma and injected mafic magma, and that little further growth occurred during subsequent ascent of the hybrid.

The situation of quartz phenocrysts sometimes exhibiting a reaction relation to melt and sometimes only resorption appears to be analogous to the situation for plagioclase phenocrysts (Browne et al., 2006a,b). Some relatively sodic plagioclase grains have a distinct "sieve" zone indicative of partial melting, surrounded by a strongly zoned overgrowth. All sodic plagioclase incorporated in mafic enclaves exhibit this texture, as do some in the host lava. Some otherwise similar plagioclase phenocrysts in the host lack sieve zones but instead contain a calcic spike at an analogous location. The sieve textured plagioclase crystals in the enclaves were apparently engulfed from host magma and "saw" a brief but intense thermal and chemical perturbation. Some of these were returned to the host when enclaves disintegrated. Non-sieved sodic plagioclase never came in contact with mafic magma, but still reflect the heating event in their zoning. Thus, pyroxene-rimmed quartz may be analogous to sieve-texture plagioclase, whereas resorbed quartz may be analogous to the non-sieve-texture sodic plagioclase of the host.

But if reaction rims only form in the extreme case of engulfment in mafic magma, why do the experiments show growth of augite

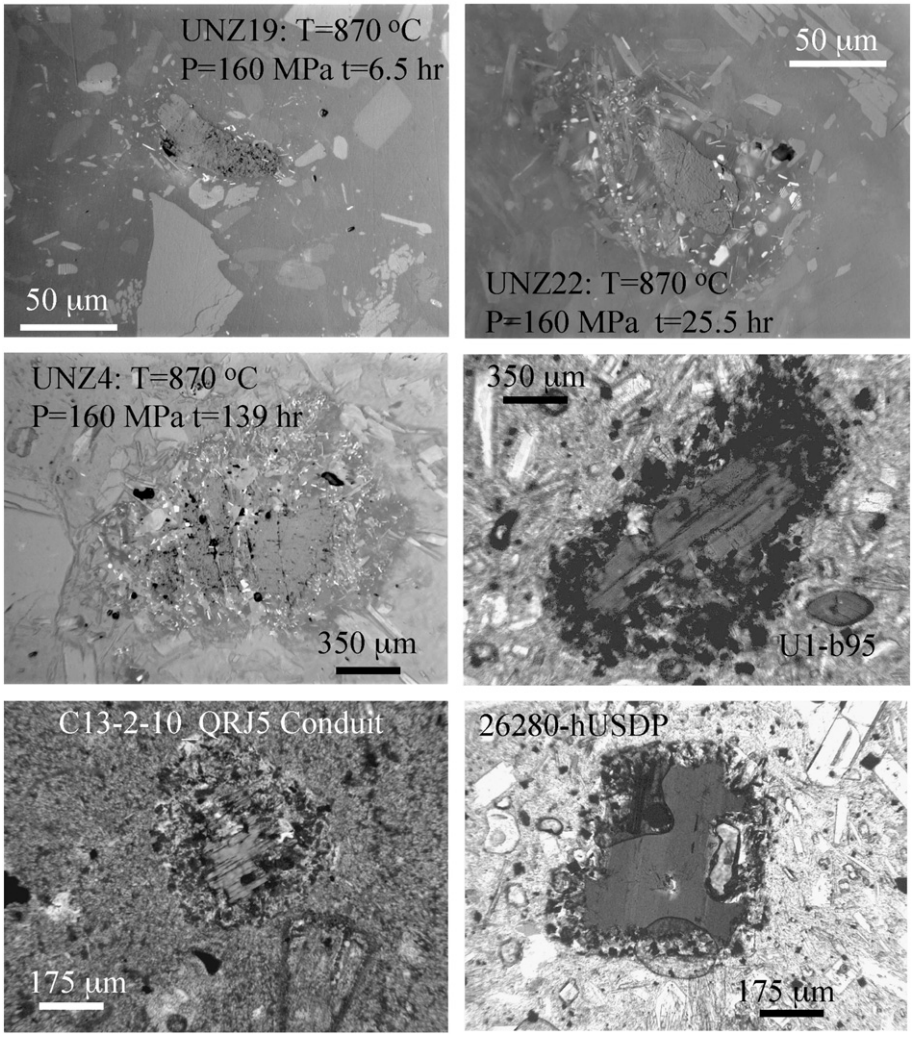

Fig. 10. These photomicrographs show development of reaction rims around biotite "seed" crystals in the heating experiments described in the text. These runs were not decompressed, but were held at the conditions listed on each image for the specified time. The U1-b95 photomicrograph shows the texture of biotite reaction rims typical in the Unzen spine lava. The bottom two photomicrographs show examples of biotite reaction rims from a conduit sample as well as from a core sample from the flanks. Here, the generally coarse rim texture on the conduit sample is apparent, when compared with that from the host lava.

reaction rims due to heating to pre-eruption temperature alone? Perhaps the heating effect inferred by Venezky and Rutherford (1999) and hence the temperature of our experiments is too high.

An alternative scenario is that reaction rims form on all quartz in Unzen magma, but are eroded off during flow in the host while protected from this erosion if encased within enclaves.

4.5.2. Biotite

Reaction rims formed around biotite phenocrysts suggest similar scenarios. Fig. 10 shows reacted biotite phenocrysts from core from the conduit, core from flank boreholes, and from the lava spine. The temperature stability limit of biotite at 160 MPa is probably similar to that of quartz (Holtz et al., 2005), yet the slope of its temperature stability curve is positive with pressure, opposite that of quartz. Thus, as the water-saturated melt is decompressed, biotite should move farther from its stability field, while the effect on quartz is opposite. Nevertheless, the experiments qualitatively show the development of reaction rims on a timescale similar to quartz.

One difference between conduit samples and experimental results is that the reaction rims seen in the conduit appear to have a slightly coarser grain size than for short experimental runs (6.5 h; Fig. 10). Although some of the biotite grains in the conduit appear only resorbed and embayed, others are almost completely reacted away, leaving a small bit of the original crystal surrounded by a coarse-grained reaction rim. The biotite reaction may have proceeded to a greater degree in the conduit because this material sat at magmatic temperatures outside the stability limit of biotite for a longer amount of time than the lava. According to Holtz et al. (2005), biotite should not be stable in the conduit at the initial emplacement temperatures of the magma at a depth of 1.3 km (Venezky and Rutherford, 1999). Thus, the differences in texture and relative width of the reaction rims between biotite in the natural lava and conduit samples may reflect the longer cooling history of the unerupted magma in the conduit.

5. Summary

We have demonstrated a chemical match between the core material intersected at 1.3 km depth and the last erupted lavas from the 1991–1995 eruption of Unzen Volcano using the REEs and other trace elements to fingerprint each. This indicates both parcels of magma belong to the same eruptive sequence, although the conduit material may represent the initial intrusion, as suggested by the low temperature, high microlite number density and small size, and plagioclase phenocrysts that do not exhibit high An rims, rather than the last-emplaced magma coincident with the final lava dome extrusion. Whether the conduit material was emplaced at the beginning of the eruption or four years later at the conclusion changes our interpretations of our findings very little. Based on the correlation of the spine and conduit as extrusive and intrusive counterparts of the same eruptive event, we are able to investigate the textural and mineralogical differences between the two to posit how the two *P–T–t* paths of this Unzen dacite have impacted the final characteristics. We find that within the conduit porosity has been reduced to a negligible volume fraction; Mg, Fe, and Na were readily mobilized due to the breakdown of hornblende and alteration of plagioclase; and C and S were introduced to the cooling magma from vapor streaming through the system. We have verified experimentally that the reaction rims seen surrounding quartz and biotite phenocrysts are indicators of the initial magma-mixing event at the on-set of eruption, and shown that biotite remained outside of its stability field for an extended period during cooling at 1.3 km.

One important conclusion, if this one drilling data point of Unzen Volcano can be taken as exemplary, is that volcanic systems can cool quickly, over the course of a decade, even when the eruption itself lasted for years. Because of this and because crystallization from both decompression as well as cooling occurred, it is unlikely that silicic magma can be stored in a magmatic state for any appreciable length of time at the base of a volcanic edifice. Current applications of this conclusion are to the renewed activity of Mount St. Helens and Augustine volcanoes where precursory seismic activity beginning at very shallow depth led to the suggestion that magma had actually been stored at that depth following their 1980s eruptive episode. Even excepting simple crystallization effects, there appear to be rapid interactions between phenocrysts and melt following the pressure perturbation of ascent that would make shallowly stored magma readily distinguishable from new magma withdrawn from a much deeper reservoir.

What is the shallow depth limit to silicic magma storage? Within a few kilometers, perhaps only 1 km, beneath the current depth of sampling at Unzen, there may be a transition to conditions under which magma could be stored for protracted periods, and where the textures of resulting intrusions become more plutonic in nature. At shallower depth than that of the Unzen conduit samples, one might see the effects of more voluminous vapor loss and development of incipient fragmentation textures. Probing volcanoes with much shorter repose periods will likely reveal an entirely different thermal regime from the thermally waning system viewed in the Unzen conduit. And one must now wonder what the conduit of a dominantly explosive andesite/dacite volcano looks like. It is to be hoped that Unzen is merely the first step in exploring volcano parameter space, in understanding the subvolcanic regime, and in understanding the relationship to eruptive behavior. The obvious next steps are to sample conduits at both greater and shallower depths than in the Unzen drilling experiment, and to also explore conduits of both more explosive and shorter repose time systems.

Acknowledgements

This research endeavor would not have been possible without the samples provided by Setsuya Nakada and the joint support of the Japan Ministry of Education, Culture, Science, Sports and Technology and the International Continental Scientific Drilling Program. The authors were supported by NSF grants EAR-0310406 and EAR-0309773. We sincerely appreciate the invaluable assistance provided by Brandon Browne, Amanda Kolker and Pavel Izbekov and the constructive manuscript reviews from H. Sato and an anonymous reviewer.

References

ASTM D513 Method B, 2002. Carbon Dioxide CO^2 Evolution, Coulometric Titration Method. ASTM International.

Ayers, J.C., Watson, E.B., 1991. Solubility of apatite, monazite, zircon, and rutile in supercritical aqueous fluids with implications for subduction zone geochemistry. Philos. Trans. R. Soc. Lond., A 335, 365–375.

Browne, B.L., Eichelberger, J.C., Patino, L.C., Vogel, T.A., Dehn, J., Uto, K., Hoshizumi, H., 2006a. Generation of porphyritic and equigranular mafic enclaves during magma recharge events at Unzen Volcano, Japan. J. Petrol. 47, 301–328. doi:10.1093/petrology/egi076.

Browne, B.L., Eichelberger, J.C., Patino, L.C., Vogel, T.A., Uto, K., Hoshizumi, H., 2006b. Magma mingling as indicated by texture and Sr/Ba ratios of plagioclase phenocrysts from Unzen volcano, SW Japan. J. Volcanol. Geotherm. Res. 154, 103–116.

Cashman, K., 1992. Groundmass crystallization of Mount St. Helens dacite, 1980–1986: a tool for interpreting shallow magmatic processes. Contrib. Mineral. Petrol. 109, 431–449.

Cashman, K., Blundy, J., 2000. Degassing and crystallization of ascending andesite and dacite. Philos. Trans. R. Soc. Lond., A 358, 1487–1513.

Cetiner, Z.S., Wood, S.A., Gammons, C.H., 2005. The aqueous geochemistry of the rare earth elements. Part XIV. The solubility of rare earth element phosphates from 23 to 150 °C. Chem. Geol. 217, 147–169.

Couch, S., Harford, C.L., Sparks, R.S.J., Carroll, M.R., 2003a. Experimental constraints on the conditions of formation of highly calcic plagioclase microlites at the Soufrière Hills Volcano, Montserrat. J. Petrol. 44, 1455–1475.

Couch, S., Sparks, R.S.J., Carroll, M.R., 2003b. The kinetics of degassing-induced crystallization at Soufrière Hills Volcano, Montserrat. J. Petrol. 44, 1477–1502.

Fulignati, P., Gioncada, A., Sbrana, A., 1998. Rare-earth element (REE) behavior in the alteration facies of the active magmatic-hydrothermal system of Vulcano (Aeolian Islands, Italy). J. Volcanol. Geotherm. Res. 88, 325–342.

Gammons, C.H., Wood, S.A., Williams-Jones, A.E., 1996. The aqueous geochemistry of the rare earth elements and Yttrium: VI. Stability of neodymium chlorite complexes from 25 to 300 °C. Geochim. Cosmochim. Acta 60, 4615–4630.

Geschwind, C., Rutherford, M.J., 1995. Crystallization of microlites during magma ascent: the fluid mechanics of recent eruptions at Mount St. Helens. Bull. Volcanol. 57, 356–370.

Hammer, J.E., Rutherford, M.J., 2002. An experimental study of the kinetics of decompression-induced crystallization in silicic melt. J. Geophys. Res. 107 (no. B1). doi:10.1029/2001JB000281.

Hammer, J.E., Cashman, K.V., Hoblitt, R.P., Newman, S., 1999. Degassing and microlite crystallization during pre-climatic events of the 1991 eruption of Mt. Pinatubo, Philippines. Bull. Volcanol. 60, 355–380.

Holtz, F., Sato, H., Lewis, J., Behrens, H., Nakada, S., 2005. Experimental petrology of the 1991–1995 Unzen dacite, Japan: Part 1: Phase relations, phase composition, and pre-eruptive conditions. J. Petrol. 46, 319–337.

Hoshizumi, H., Uto, K., Watanabe, K., 1999. Geology and eruptive history of Unzen Volcano, Shimabara Peninsula, Kyushu, SW Japan. J. Volcanol. Geotherm. Res. 89, 81–94.

Klug, C., Cashman, K.V., 1994. Vesiculation of May 18, 1980, Mount St. Helens magma. Geology 22, 468–472.

Klug, C., Cashman, K.V., Bacon, C.R., 2002. Structure and physical characteristics of pumice from the climactic eruption of Mount Mazama (Crater Lake), Oregon. Bull. Volcanol. 64, 486–501. doi:10.1007/s00445-002-0230-5.

Liu, M., Yund, R.A., 1992. NaSi-CaAl interdiffusion in plagioclase. Am. Mineral. 77, 275–283.

Moore, G., Carmichael, I.S.E., 1998. The hydrous phase equilibria (to 3 kbar) of an andesite and basaltic andesite from western Mexico: constraints on water content and conditions of phenocryst growth. Contrib. Mineral. Petrol. 130, 304–319.

Nakada, S., Motomura, Y., 1999. Petrology of the 1991–1995 eruption at Unzen: effusion pulsation and groundmass crystallization. J. Volcanol. Geotherm. Res. 89, 173–196.

Nakamura, M., 1995. Continuous mixing of crystal mush and replenished magma in the ongoing Unzen eruption. Geology 23, 807–810.

Nishimura, K., Kawamoto, T., Kobayashi, T., Sugimoto, T., Yamashita, S., 2005. Melt inclusion analysis of the Unzen 1991–1995 dacite: implications for crystallization processes of dacite magma. Bull. Volcanol. 67, 648–662.

Polacci, M., Pioli, L., Rosi, M., 2003. The Plinian phase of the Campanian Ignimbrite eruption (Phlegrean Fields, Italy): evidence from density measurements and textural characterization of pumice. Bull. Volcanol. 65, 418–432.

Riehle, J.R., 1973. Calculated compaction profiles of rhyolitic ash-flow tuffs. Geol. Soc. Amer. Bull. 84, 2193–2216.

Sakuma, S., Kajiwara, T., Nakada, S., Uto, K., Shimizu, H., 2008. Drilling and logging results of USDP-4. - Penetration into the volcanic conduit of Unzen Volcano, Japan -. J. Geophys. Res. 175, 1–12 (this issue). doi:10.1016/j.jvolgeores.2008.03.039.

Sun, S., McDonough, W.F., 1989. Chemical and isotopic systematics of oceanic basalts: implications for mantle compositions and processes. In: Norry, M.J. (Ed.), Magmatism in the Ocean Basins. Geological Society Special Publications, pp. 313–345.

Thomas, N., Jaupart, C., Vergniolle, S., 1994. On the vesicularity of pumice. J. Geophys. Res. 99, 15633–15644.

Venezky, D.Y., Rutherford, M.J., 1999. Petrology and Fe–Ti oxide reequilibration of the 1991 Mount Unzen mixed magma. J. Volcanol. Geotherm. Res. 89, 213–230.

Vogel, T.A., Flood, T.P., Patino, L.C., Maximo, R.P.R., Arpa, C.B., Arcilla, C.A., Stimac, J.A., 2006. Geochemistry of silicic magmas in the Macolod Corridor, SW Luzon Philippines: evidence of distinct, mantle-derived, crustal sources for silicic magmas. Contrib. Mineral. Petrol. 151, 267–281.

Wood, S.A., Williams-Jones, A.E., 1994. The aqueous geochemistry of the rare-earth elements and Yttrium. IV. Monazite solubility and REE mobility in exhalative massive sulfide-depositing environments. Chem. Geol. 115, 47–60.